Longitudinal Leaky SAW Resonators and Filters on YZ-$LiNbO_3$

Tapani Makkonen[1,2], Victor P. Plessky[3], William Steichen[2], Valeri I. Grigorievski[4], Marc Solal[2], and Martti M. Salomaa[1]

[1]Materials Physics Laboratory, Helsinki University of Technology,
P.O. Box 2200, FI-02015 TKK, Finland
[2]TEMEX, 06904 Sophia Antipolis, France
[3]GVR Trade SA, CH-2022 Bevaix, Switzerland
[4]Institute of Radioengineering and Electronics of the Russian Academy of Sciences,
Moscow 103907, Russia

***Abstract*— The high phase velocity (above 6100 m/s in an Al grating on $LiNbO_3$) of the longitudinal leaky SAW (LLSAW) mode makes it attractive for application in high frequency SAW ladder filters in the 2–5 GHz range. We investigate the dependence of one-port synchronous LLSAW resonator performance on YZ-$LiNbO_3$ on the metallization thickness and metallization ratio, both experimentally and theoretically. Our results indicate a strong dependence of the Q factor and resonance frequency on the aluminum thickness, with the optimal thickness that produces the highest Q values being about 8%. The optimal thickness increases with the metallization ratio. The observed behavior is interpreted with the help of simulations using a combined FEM/BEM method. As an application, bandpass filters have been fabricated in the 2.8 GHz frequency regime, based on longitudinal leaky SAWs. The synchronous resonators constituting the ladder filters operate in the fundamental mode. The filters feature low insertion losses below 3 dB and wide relative passbands of 4.5–5%.**

I. Introduction

LONGITUDINAL leaky (LL) waves propagating in a periodic system of Al electrodes on YZ-$LiNbO_3$ (LN) substrate surface feature high velocities (above 6100 m/s [1], [2]), enabling conventional optical lithography to be used in the fabrication of the LLSAW filters for the 2–5 GHz frequency range. Several wireless communication standards, such as Bluetooth (2.45 GHz) and HiperLAN (5.25 GHz), operate in this frequency range. LLSAW on YZ-LN features strong coupling (resonance-antiresonance distance (R-a-R) close to 4.5%) and low losses, rendering it a suitable propagation mode for the realization of high-frequency wide-band low-loss filters.

The velocity of the LLSAW mode is between those of the fast quasi-shear and quasi-longitudinal bulk-acoustic waves (BAW). For YZ-LN, the LLSAW velocity is about twice the velocity of the Rayleigh SAW. The LLSAW mode propagating in a grating of Al electrodes on YZ-LN is depicted in Fig. 1. The propagation direction is along the crystal Z axis, while the surface normal is along the crystal Y axis. The shear bulk wave with its displacement component perpendicular to the sagittal plane (YZ plane) is decoupled and the displacement of the LLSAW is in the sagittal plane. Hence, only one of the two partial modes constituting the SAW solution in the substrate exhibit bulk characteristics [3]. This partial mode corresponds to the shear bulk wave which radiates power into the substrate and is responsible for the propagation loss. The dominant surface-displacement component for LLSAW is in the propagation (crystal Z) direction.

To satisfy the stressfree boundary condition, a wave propagating along a free surface of an isotropic elastic half-space is composed of two strongly coupled partial waves, the shear and the longitudinal wave. Due to this coupling, a longitudinal wave propagating along the surface would radiate all its energy in the form of shear waves into the substrate within a distance comparable to a single wavelength. The first

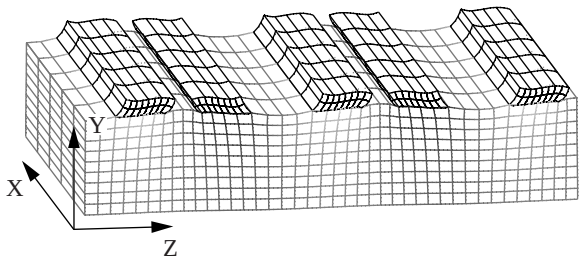

Fig. 1. LLSAW propagating in a periodic system of Al electrodes on YZ-LN. The shades of gray in the substrate indicate the displacement component in the propagation direction (crystal Z direction). The electrodes are drawn with black lines. For the illustration purposes the displacements are exaggerated.

discussion of this kind of surface resonance was given by Glass and Maradudin [4]. They found that LL waves propagating in an isotropic elastic half-space with a free surface feature very high propagation losses, on the order of a few dB/λ on a flat surface. The loss was found to decrease slightly for a corrugated surface, but it was still too high to enable any practical applications. Sato and Abe applied the LLSAW mode on lithium tetraborate (LBO) to implement bandpass filters (of the interdigitated interdigital transducer type) in the 1.5 GHz frequency range [5]. On LBO, the propagation loss of LLSAW is low for both free and metallized (flat) surfaces [6], as well as for surfaces covered with a periodic Al grating [7]. Kobayashi et al. reported experimental LLSAW resonators on LN and $LiTaO_3$ substrates [8] as well as LLSAW ladder filter on $LiTaO_3$ with center frequency around the 1.9 GHz frequency range [9]. Isobe et al. have investigated LLSAW properties in cuts of LN and $LiTaO_3$ using FEM modeling of an infinite periodic transducer structure [2]. It was found that a relatively high thickness of Al electrodes ($\approx$8%) is necessary for achieving low propagation losses. In particular, Grigorievski [1] has studied LLSAW on the YZ-cut of LN, showing with numerical simulations that the propagation loss of LLSAW on a flat metallized surface is high, on the order of 1.5 dB/λ. However, in a periodic system of Al electrodes with relative thicknesses close to 8%, the propagation loss is quite low.

The low propagation loss is attributed to the presence of the Al electrode grating, which modifies the boundary condition on the substrate surface. This mechanism is similar to that described, e.g., by Darinskii et al. [10], in connection with their theoretical study of LLSAW propagating in a structure composed of a uniform thin film on a substrate: The longitudinal and shear partial waves are coupled in the substrate through the materials constants and the boundary condition on the surface. The thin-film layer on the substrate also couples the partial waves. There may exist a layer thickness for which these two contributions exactly compensate each other. This results in a decoupling of the longitudinal and shear partial waves, such that in the substrate the wave is composed only of the longitudinal partial wave, whose mechanical displacement decays exponentially into the substrate. In this case, the LLSAW mode turns into a proper SAW propagating without attenuation [11], [12]. Apparently, the periodic Al grating similarly modifies the boundary condition at the surface of the YZ-LN substrate in such a way that the coupling to the shear bulk wave becomes weak, although it does not completely vanish. Plessky et al. [13] proposed that this effect is a consequence of the Al electrodes acting as a periodic system of $\lambda/4$ resonators on the LN surface, where λ is the shear wavelength in Al. Gulyaev et al. attributed the relatively low attenuation of LLSAW on YZ-LN to the presence of hybrid LLSAW-BAW modes [14].

In this paper, we investigate in detail the dependence of synchronous LLSAW resonator preformance on the Al electrode geometry, fabricated on a YZ-cut LN substrate. We concentrate on the YZ-LN since it is widely used, readily available, not strongly pyroelectric, and it does not exhibit beam steering. In Section II, we present results on numerical FEM/BEM [15] simulations of infinite periodic transducers for different electrode thicknesses and metallization ratios. In addition, simulations of the admittance response for one-port synchronous LLSAW resonators are carried out using the FEM/BEM method for finite structures [16] to analyze the effects of mass loading on the resonance frequencies and Q values. The experimental results for LLSAW resonators are presented in Section III. The performance of fabricated prototype LLSAW filters is reported in Section IV. Section V provides a discussion of the results, followed by conclusions in Section VI.

II. Simulations

A. Modeling an Infinite Periodic IDT on YZ-LN

SAW devices often comprise of long periodic electrode gratings. Hence, an understanding of the propagation characteristics of the different SAW modes in such structures is useful for the optimization of the device performance. Considering that LLSAW radiates energy into the substrate in the form of shear bulk waves, the emphasis is on the minimization of the propagation losses.

To explore the propagation properties of LLSAWs in a substrate loaded with a periodic Al strip grating, the harmonic admittance of an infinitely long periodic interdigital transducer (IDT) structure is computed, employing the FEM/BEM[1] with phased-periodic boundary conditions [15]. The Q values at resonance ($Q_{\rm r}$) and at antiresonance ($Q_{\rm ar}$) are determined from the conductance and resistance resonance peaks, respectively, as $f_{\rm p}/\Delta f$, where $f_{\rm p}$ is the peak frequency, and Δf is the full width at half-maximum of the peak. The resonance ($f_{\rm r}$) and antiresonance ($f_{\rm ar}$) frequencies are obtained as the frequencies of maximum conductance and maximum resistance, respectively. The materials constants for LN used in our simulations are taken from Ref. [17].

The calculated resonance frequencies are displayed in Fig. 2 as functions of the normalized Al thickness (h/λ_0 parameter) for different metallization ratios (a/p parameter). It is seen that the sensitivity of the resonance frequency to the metallization thickness is stronger than to a/p and that the sensitivity to thickness increases with decreasing a/p.

The Q factors at resonance and at antiresonance as functions of the relative Al thickness with a/p as the parameter are plotted in Fig. 3. Both $Q_{\rm r}$ and $Q_{\rm ar}$ feature a strong dependence on h/λ. In the simulation, several loss mechanisms, such as resistive losses and acoustic losses in the electrodes, are neglected. The resistive losses are expected to be more significant for low a/p. Note that, for a/p=0.3–0.35, the lowest losses both at resonance and at antiresonance occur for the same Al thickness.

[1]The electrodes are modeled using FEM and the substrate using a Green's-function formalism. At the interface, the two are connected using the boundary element method (BEM).

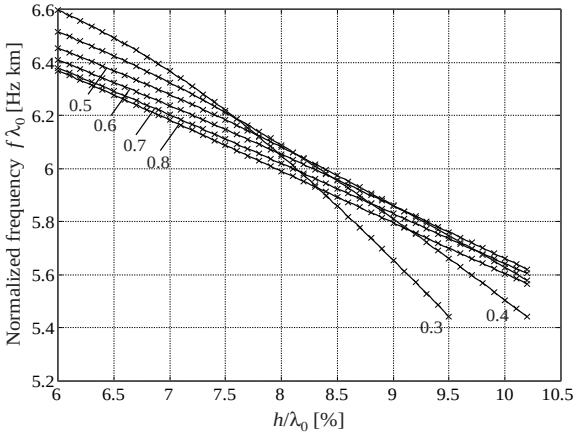

Fig. 2. Simulated normalized resonance frequency for an infinite periodic IDT as a function of h/λ_0, with the metallization ratio varying between 0.3 and 0.8.

TABLE I
GEOMETRICAL PARAMETERS FOR THE SIMULATED AND MEASURED RESONATORS.

Parameter	Simulation	Experiment (at 1.6 GHz)
pitch	1.064 μm	2 μm
metallization ratio	0.35–0.70	0.4–0.7
metallization thickness	7.2–8.8%	7–10%
aperture	30 μm	51 μm
# of fingers in IDT	301	151
# of fingers in (shorted) reflectors	20	37

B. Simulations of Synchronous LLSAW Resonators

Owing to the high attenuation of LLSAW on a flat surface of YZ-LN, the utilization of LLSAW requires strictly periodic electrode configurations, as is the case for synchronous resonators. A FEM/BEM software for finite structures [16] is used to study the resonance behavior of one-port synchronous LLSAW resonators on YZ-LN. The model accounts also for the resistive losses. The geometry of the resonators used in the simulations is summarized in Table I.

The simulated admittance vs. frequency for different Al thicknesses and a/p is plotted in Figs. 4 and 5, respectively. We want to point out that the results presented here are more precise than those reported earlier in Ref. [18] due to improved numeric simulation procedures. From

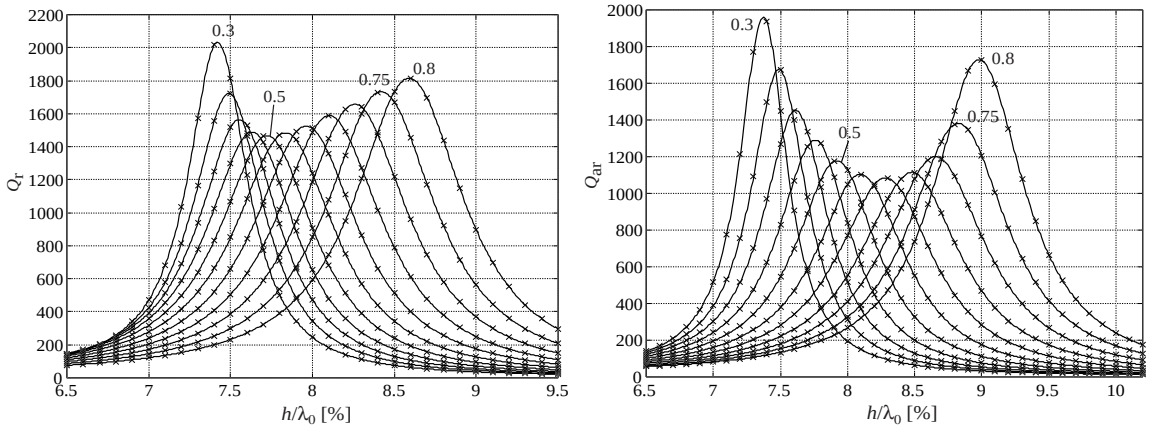

(a) (b)

Fig. 3. Simulated Q factors (a) at resonance and (b) at antiresonance for an infinite periodic IDT as functions of h/λ_0, with a/p varying from 0.3 to 0.8 with a step of 0.05. The crosses and solid curves indicate computed points and interpolated values, respectively.

Fig. 5, it is seen that the simulation predicts that for h/λ=7.8% and a/p=0.45–0.50, the resonance and antiresonance frequencies are insensitive to small variations of a/p. This is confirmed by Fig. 6, where both the simulated and measured normalized resonance and antiresonance frequencies are plotted as functions of a/p. Since the simulations were carried out for a resonator with a higher operating frequency than that of the measured resonators, a normalized frequency is used in the plot. Note that results simulated for synchronous resonators are for h/λ_0=7.8%, while all the other results are for the slightly different Al thickness of 8%. It can be seen from Fig. 6 that the simulated and measured resonance frequencies agree well, while the measured antiresonance frequencies are lower than those simulated. The larger simulated resonance-antiresonance distance—in comparison with the measured one—is attributed to an underestimation of the capacitance in the simulation. In the test resonator there are stray capacitances, e.g., due to the capacitance between the busbars and the capacitances between the ends of the fingers and the busbar. The correction to the value of the static capacitance for simulations may be estimated from the measured test resonator admittances.

The simulated Q values vs. h/λ_0 are displayed in Fig. 7. The Q at resonance for a/p=0.6, simulated using a model for an infinite IDT, features a maximum for an Al thickness

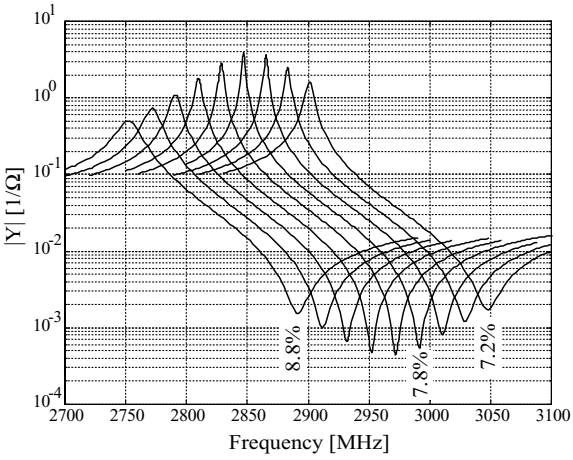

Fig. 4. Simulated admittances for synchronous LLSAW resonators (a/p=0.60) with h/λ_0 varying from 7.2% to 8.8% with increments of 0.2%.

of 8.0%, whereas in the finite FEM/BEM simulation the largest Q occurs at about 7.8%. The simulations suggest that, in general, the $Q_{\rm ar}$ is maximized for a higher Al thickness than what is required for maximizing $Q_{\rm r}$.

III. LLSAW Test Resonators

The LLSAW resonator characteristics have been studied experimentally by measuring (on wafer) the admittance response of one-port synchronous LLSAW resonators fabricated on the YZ-LN substrate. We consider both 1:1 and 1:3 IDT configurations. In the latter case, each finger connected to one busbar is followed by three

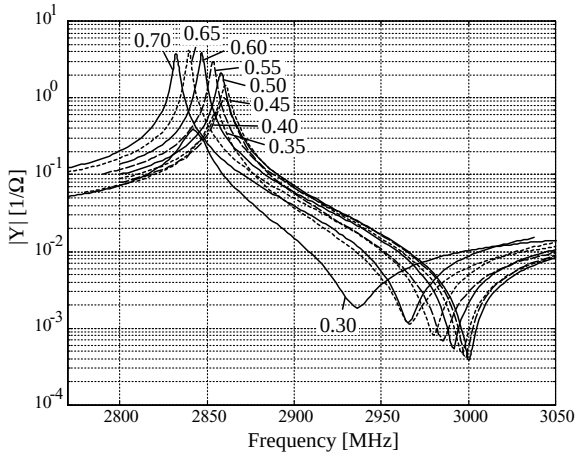

Fig. 5. Simulated admittances for synchronous LLSAW resonators (h/λ_0=7.8%) with a/p as a parameter.

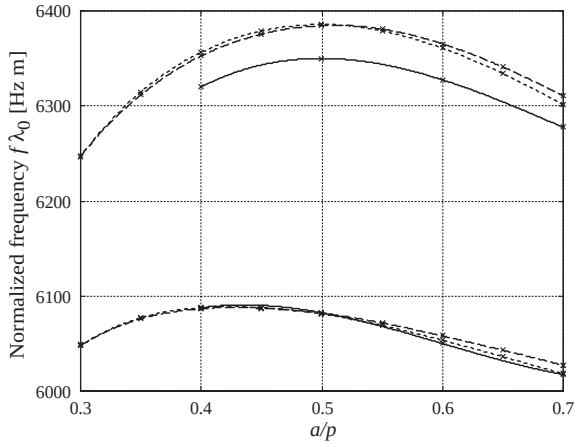

Fig. 6. Normalized resonance (lower curves) and antiresonance (upper curves) frequencies vs. a/p. Dashed lines: simulated using FEM/BEM for finite structures, h/λ=7.8%; dotted lines: simulated using periodic FEM/BEM, h/λ=8.0%; solid lines: measured, h/λ=8.0%, at the 1.6 GHz range of frequencies.

fingers connected to the opposite busbar. Due to the strong coupling of the LLSAW on YZ-LN, the 1:1 structures can be used for filters with a 4–5% bandwidth. Resonators with the 1:3 electrode configuration are useful in applications where a filter bandwidth of about 2% is needed.

A. 1:1 IDT Resonators

The structural parameters of the test resonators operating in the 1.6 GHz range of frequencies are listed in Table I. Figure 8 displays the dependence of the experimental resonance and antiresonance frequencies on the thickness

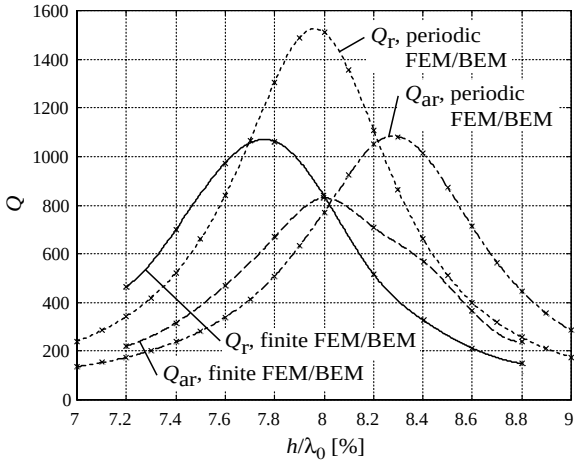

Fig. 7. Simulated Q values at resonance and antiresonance vs. h/λ_0 for a 1:1 electrode configuration. All for a/p=0.60. The computed points are denoted with crosses, the continuous curves were interpolated using cubic splines.

of the electrodes for different a/p. Also shown are the frequencies simulated for a/p = 0.6 with the FEM/BEM method for finite structures. The measured dependence of resonance frequencies on h/λ for a/p = 0.60 is in agreement with the simulation. Qualitatively, the measured behavior in Fig. 8 also agrees with the simulated behavior for an infinite IDT in Fig. 2.

The 1.6 GHz test resonator has also been studied with a scanning Michelson laser interferometer. The magnitude of the surface-displacement component in the Y-direction within the resonator has been measured using the interferometer at different frequencies around the resonance frequency and the results are reported in Ref. [19].

The temperature coefficient of frequency for LLSAW in Al electrode gratings on YZ-LN is rather high; the experimental value of -105 ppm/K (for $a/p = 0.7$, $h/\lambda = 8.0\%$) is reported in Ref. [20]. This somewhat offsets the wide filter bandwidth achievable using LLSAW, since part of the band has to be sacrificed to temperature variations.

Figure 9 displays the Q values at resonance and at the antiresonance as a function of the electrode thickness for different metallization ratios, determined from the measured admittances of test resonators in the 2.8 GHz frequency range. Q_r values over 300 are measured. The variation in the Q values for resonators which have the

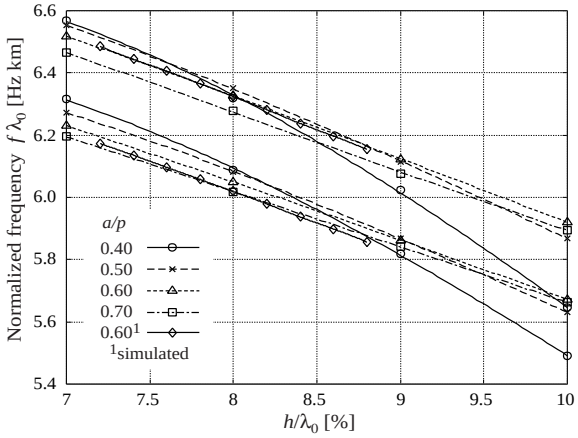

Fig. 8. Measured normalized resonance (lower curves, $\lambda_0 f_{\rm r}$) and antiresonance frequencies (upper curves, $\lambda_0 f_{\rm ar}$) vs. h/λ_0 for different a/p. The results are measured on test resonators in the 1.6 GHz frequency range. Symbols denote experimental and simulated values, lines are a cubic spline interpolation.

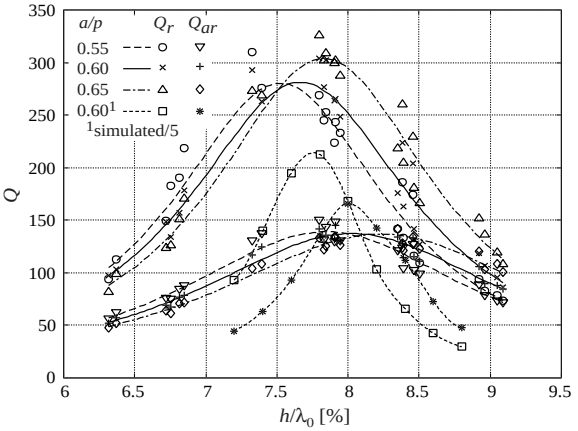

Fig. 9. Measured Q at resonance (upper curves) and at antiresonance (lower curves) vs. h/λ_0 for different a/p determined from test resonators with 1:1 IDT in the 2.8 GHz frequency range. For the simulated values, the curves are cubic spline interpolations. For the experimental values, the curves are parabolas fitted to the measurements.

same metallization thickness is due to the differences in the aperture and the number of fingers in the IDT. To facilitate qualitative comparison between the simulation and measurement, the simulated Q values have been multiplied by a factor of 0.20. The simulated and measured Al thicknesses providing the highest Q at resonance for a/p = 0.6 agree well, being about 7.8% and 7.7%, respectively. In agreement with theory, the optimum thickness for the highest Q increases with a/p. Considering resistive losses in the electrodes, the relatively large optimum finger thickness is advantageous at high frequencies, since the electrode resistivity increases with decreasing electrode thickness. The experimental Q values are much lower than the computed ones, partly because the mechanical losses in the electrodes, the intrinsic losses in the substrate and the contact resistances present in the measurements are omitted in the simulations. It is likely that electrical losses in the electrodes are also underestimated. It is seen in Fig. 1 that the deformations in the electrodes are large. This is supposed to result in increased contribution of viscous damping in the electrodes to the losses.

Qualitatively, both measurement and theory show that the highest attainable Q at antiresonance is lower than that attainable at resonance. However, the measured difference between $Q_{\rm r}$ and $Q_{\rm ar}$ is larger than the difference predicted by theory.

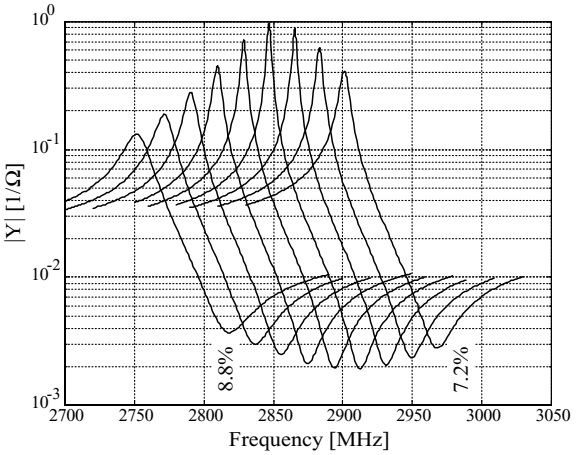

Fig. 10. Simulated admittances for the 1:3 IDT resonators (a/p=0.60) with h/λ_0 varying from 7.2% to 8.8% with a step of 0.2%.

B. 1:3 IDT Resonators

The computed admittance curves for a resonator with 1:3 IDT structure for different h/λ and different a/p are shown in Figs. 10 and 11, respectively. Comparing the simulated admittance curves for the 1:1 and 1:3 resonators, it is seen that the Q value at antiresonance is clearly lower for the 1:3 resonator. The 1:1 configuration also exhibits a larger difference between the magnitudes of the admittances at resonance and antiresonance than the 1:3 configuration.

Figure 12 displays the Q values at resonance and at antiresonance as a function of the elec-

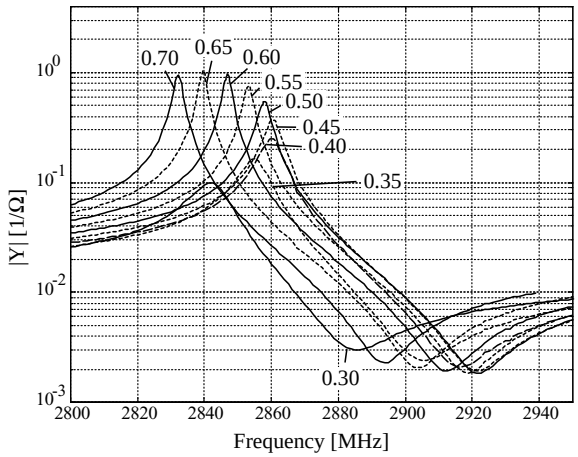

Fig. 11. Simulated admittances for the 1:3 IDT resonators (h/λ_0=7.8%) with a/p as a parameter.

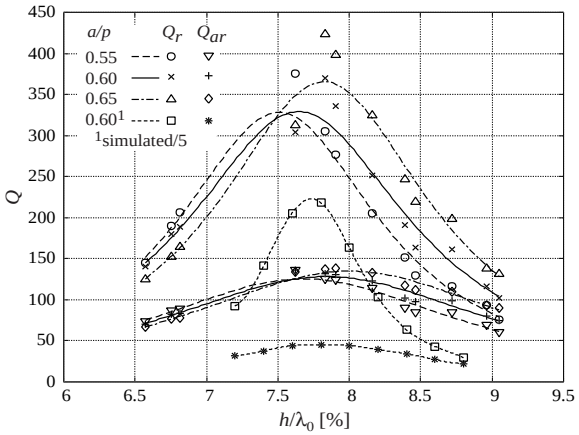

Fig. 12. Measured Q at resonance (upper curves) and at antiresonance (lower curves) vs. h/λ_0 for different a/p determined from test resonators with 1:3 IDT in the 2.8 GHz frequency range. For the simulated values, the curves are cubic spline interpolations. For the experimental values, the curves are parabolas fitted to the measurements.

trode thickness for different metallization ratios, determined from the measured admittances of the test resonators with 1:3 IDT structure in the 2.8 GHz frequency range. The highest measured $Q_{\rm r}$ value is over 400, i.e., even higher than that for the 1:1 IDT resonators. The simulated $Q_{\rm ar}$ values for the 1:1 configuration are about a factor of three higher than those for the 1:3 configuration, although the measured values are approximately equal. The reasons underlying these discrepancies remain to be studied in greater detail.

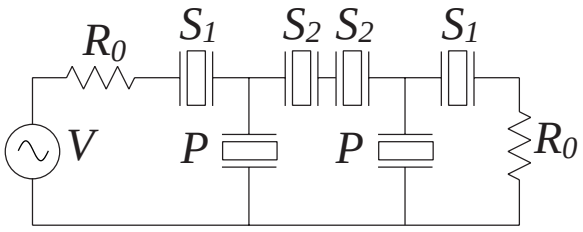

Fig. 13. Electrical connection of the LLSAW resonators in the prototype ladder filter. Here, V and R_0 denote the source voltage and source/load resistance, respectively.

IV. LLSAW Filters

The simulated and measured results for LLSAW resonators serve to indicate that LLSAW on YZ-LN with thick electrodes possesses characteristics suitable for the realization of low-loss ladder filters in the 2–5 GHz frequency regime. To demonstrate the filter performance achievable using the LLSAW resonators, we here report results for LLSAW ladder filters with a center frequency in the 2.8 GHz frequency range. Filters for 2.5 GHz [21], [22] and 5.25 GHz [22], [23] have also been fabricated, with the latter demonstrating the feasibility of employing the LLSAW mode on YZ-LN to implement filters for 5 GHz frequencies using conventional optical lithography.

The electrical interconnection of the individual LLSAW resonators in the 2.8 GHz ladder filters is displayed in Fig. 13. The geometrical parameters of the series and parallel resonators in the filter are summarized in Table II. The series resonator has a lower pitch than the parallel resonator and, consequently, a higher relative metallization thickness. It is seen in Fig. 9 that the maximum Q at resonance and at antiresonance occur for different metallization thicknesses. For low IL at the center frequency, it would be desirable to have a high Q at both the resonance of the series resonator and at the antiresonance of the parallel resonator. For this purpose, one might utilize the fact that the relative thickness providing the highest Q decreases with a/p and use a lower a/p in the parallel resonator than in the series resonator.

The details of the transmission response in the passband measured for the prototype filter are displayed in Fig. 14, together with the group delay. It can be observed that the passband is reasonably smooth and the group delay variation

TABLE II

GEOMETRICAL PARAMETERS FOR THE SERIES AND PARALLEL RESONATORS OF THE 2.8 GHZ LLSAW LADDER FILTER.

	Resonator		
Parameter	S_1	S_2	P
pitch	1.100 μm	1.070	1.150 μm
metallization ratio	0.60	0.60	0.60
aperture	25.5 μm	25.5 μm	25.5 μm
# of fingers in IDT	267	221	233
# of fingers in (shorted) reflectors	37	37	37

S_1: series resonators closest to the input and output
S_2: middle series resonators; P: parallel resonators

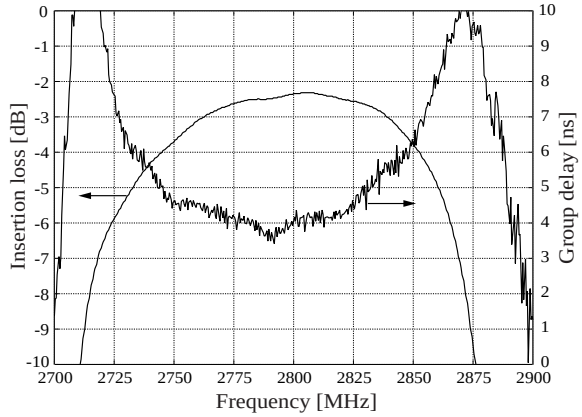

Fig. 14. Measured insertion loss and group delay vs. frequency in the passband for the LLSAW ladder filter. The Al thickness is 1700 Å and a/p=0.60.

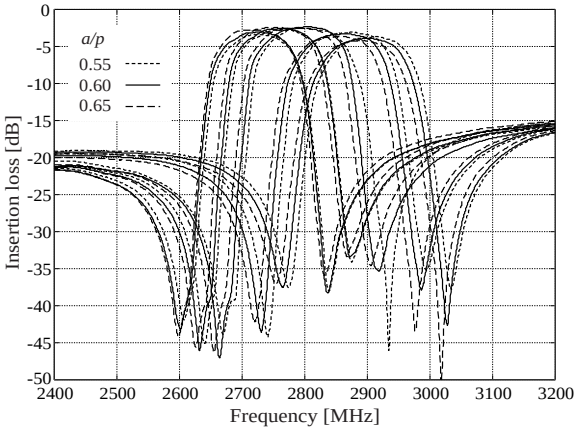

Fig. 15. Measured insertion loss vs. frequency for LLSAW ladder filters for Al thicknesses 1945 Å, 1820 Å, 1700 Å, 1565 Å and 1465 Å (from left to right). For each Al thickness, there are three curves for a/p = 0.55, 0.60 and 0.65.

is on the order of 1 ns at the middle of the passband. The lowest insertion loss is 2.3 dB, the center frequency is 2796 MHz and the 3 dB bandwidth is 132.5 MHz (fractional bandwidth 4.7%). The rounded shape of the passband indicates that the bandwidth may be even further widened by increasing the frequency shift between the series and parallel resonators. The bandwidth is also limited by the rounded edges of the passband. Sharper cut-off characteristics would require higher resonator Q values.

The influence of the Al thickness and metallization ratio of the resonators on the filter transmission characteristics is shown in Fig. 15. It is clearly seen that the center frequency of the filter is significantly more sensitive to the metallization thickness than to the metallization ratio. The suppression level on the upper stopband is only moderate, 15 dB. In ladder filters, the stopband suppression level may be improved by increasing the capacitance ratio between the series and parallel resonators or using more sections in series [24]. However, this also results in an increase in the insertion loss in the passband.

The YZ-LN also supports the Rayleigh SAW mode; for an Al grating with normalized thickness 7.8% and a/p=0.50, the calculated velocity (resonance frequency times grating wavelength) is 3297.7 m/s. Consequently, there exists a spurious passband in the filter response arising from the Rayleigh SAW at about half the frequency of the LLSAW passband [23]. Depending on the application, measures to suppress this spurious passband may be needed.

V. DISCUSSION

The main reason underlying the difference between the Q values shown in Fig. 7 computed

with the finite and periodic FEM/BEM tools is considered to be the neglect of the electrical losses within the periodic FEM/BEM, although taken into account in the finite FEM/BEM. Futhermore, the two simulations have different computational parameters, e.g., the number of nodes in the FEM model of the electrode, which may cause slight differences between the results computed using the two methods. It is also known that the bulk wave radiation is stronger for finite structure than for an ideal periodic infinite structure, resulting in a correspondingly lower Q value for the finite structure. Although the periodic FEM/BEM may be employed to obtain an estimate for the admittance of a long IDT, the results of the finite FEM/BEM simulations are more accurate in predicting the performance of the actual LLSAW resonators.

The 3–4 times higher simulated Q in comparison with the measured Q in Figs. 9 and 12 is attributed to an underestimation of the electrical losses in the simulation and, foremost, to the omission of viscous losses in the electrodes in the simulation. The mechanical losses may be represented in the simulation, e.g., by using a complex stiffness matrix for Al [25]. Due to the large strains in the electrodes associated with the propagating LLSAW (see Fig. 1), the mechanical losses are considered to constitute a significant loss mechanism.

The Al fingers act as periodic resonators attached to the LN surface and coupled through the LN substrate, resulting in decreased coupling to the shear bulk partial wave in the substrate. The idea was confirmed by Solal et al. [26]: they demonstrated theoretically and experimentally that the propagation of LL-waves is also allowed for Al fingers with thickness about three times higher than the value close to 8% required here for the highest resonator Q values. They showed that the optimum electrode thicknesses providing low propagation loss for the LLSAW are related to wavelength of the flexure wave in the electrodes. FEM/BEM simulations also predict that the LL-waves exist in split finger configurations (in IDTs with 4 electrodes per electrical period), showing strong resonance properties [26]. Hence, the strong reflections and the Bragg stopband observed in standard 1:1 IDTs are not necessary for the existence of LL-waves. However, a study of these topics is beyond the scope of the present paper.

VI. Conclusions

We have investigated the effects of Al electrode thickness and metallization ratio on the LLSAW propagation properties under electrode gratings on a YZ-LN substrate using a model for an infinite periodic transducer. In addition, the dependence of the performance of synchronous one-port LLSAW resonators on YZ-LN on the Al electrode dimensions is simulated. Both the 1:1 and 1:3 IDT configurations are considered. Measured data on the dependence of the Q factor and resonance frequencies of LLSAW resonators on the Al thickness and metallization ratio has also been presented. Both simulations and measurements indicate that an Al thickness of about 8% is required to maximize the resonator Q values.

For resonators with the 1:1 IDT configuration, operating in the 2.8 GHz frequency range, Q values over 300 have been measured at resonance, while the Q at antiresonance is found to be about half this value. The Q values and resonance frequencies are found to depend rather strongly on the metallization thickness. The optimum Al thickness which ensures for the lowest loss at antiresonance is larger than the optimum thickness for the lowest loss at resonance; the difference between these two optimal thicknesses increases with a/p.

The LLSAW is applied to realize bandpass filters with center frequencies in the 2.8 GHz frequency range. The prototype ladder filter, composed of synchronous one-port LLSAW resonators, features a minimum loss of 2.3 dB, a wide fractional 3 dB bandwidth of 4.7% and a 15 dB stopband rejection. Hence, LLSAW renders possible the mass fabrication of low-loss wide-band filters for wireless communication standards within the 2–5 GHz frequency range using just conventional optical lithography.

Acknowledgement

Cedric Poirel and other colleagues at TEMEX are acknowledged for the fabrication of the test resonators and filters. We are grateful to our colleagues at École Polytechnique, Centre de Mathématiques Appliquées for the development of the FEM/BEM simulation software for finite

structures employed in the filter design. T. Makkonen acknowledges Nokia Foundation and the Finnish Cultural Foundation for scholarships. This research has been carried out within the Eureka project E! 2442 SUMO.

REFERENCES

[1] V. I. Grigorievski, "Fast leaky surface acoustic waves on lithium niobate and lithium tantalate", in *Proc. IEEE Ultrasonics Symposium*, 2000, pp. 259–262.

[2] A. Isobe, M. Hikita, and K. Asai, "Propagation characteristics of longitudinal leaky SAW in Al-grating structure", *IEEE Trans. Ultrason., Ferroelect., Freq. Contr.*, vol. 46, pp. 849–855, 1999.

[3] M. P. da Cunha, "High velocity pseudo surface waves (HVPSAW): Further insight", in *Proc. IEEE Ultrasonics Symposium*, 1996, pp. 97–106.

[4] N. E. Glass and A. A. Maradudin, "Leaky surface-elastic waves on both flat and strongly corrugated surfaces for isotropic, nondissipative media", *J. Appl. Phys.*, vol. 54, pp. 796–805, 1983.

[5] T. Sato and H. Abe, "SAW device applications of longitudinal leaky surface waves on lithium tetraborate", *IEEE Trans. Ultrason., Ferroelect., Freq. Contr.*, vol. 45, pp. 1506–1516, 1998.

[6] T. Sato and H. Abe, "Propagation properties of longitudinal leaky surface waves on lithium tetraborate", *IEEE Trans. Ultrason., Ferroelect., Freq. Contr.*, vol. 45, pp. 136–151, 1998.

[7] T. Sato and H. Abe, "Propagation of longitudinal leaky surface waves under periodic metal grating structure on lithium tetraborate", *IEEE Trans. Ultrason., Ferroelect., Freq. Contr.*, vol. 45, pp. 394–408, 1998.

[8] Y. Kobayashi, Y. Hirao, K. Takeuchi, T. Usuki, K. Shibata, and Y. Shimizu, "New high-phase-velocity leaky surface acoustic wave mode on $LiTaO_3$ and $LiNbO_3$", *Jpn. J. Appl. Phys.*, vol. 34, pp. L1309–L1310, 1995.

[9] Y. Kobayashi, N. Tanaka, K. Matsui, H. Okano, T. Usuki, and K. Shibata, "1.9 GHz-band surface acoustic wave device using second leaky mode on $LiTaO_3$", *Jpn. J. Appl. Phys.*, vol. 35, pp. 2987–2990, 1996.

[10] A. N. Darinskii, I. S. Didenko, and N. F. Naumenko, ""Fast" quasilongitudinal sagittally polarized surface waves in layer-substrate structures", *J. Acoust. Soc. Amer.*, vol. 107, pp. 2351–2359, 2000.

[11] I. S. Didenko, F. S. Hickernell, and N. F. Naumenko, "The experimental and theoretical characterization of the SAW propagation properties for zinc oxide films on silicon carbide", *IEEE Trans. Ultrason., Ferroelect., Freq. Contr.*, vol. 47, pp. 179–187, 2000.

[12] N. F. Naumenko and I. S. Didenko, "High-velocity surface acoustic waves in diamond and sapphire with zinc oxide film", *Appl. Phys. Lett.*, vol. 75, pp. 3029–3031, 1999.

[13] V. Plessky, T. Makkonen, and M. M. Salomaa, "Leaky SAW in an isotropic substrate with thick electrodes", in *Proc. IEEE Ultrasonics Symposium*, 2001, pp. 239–242.

[14] Y. V. Gulyaev, V. I. Grigorievski, and V. P. Plessky, "Longitudinal leaky surface acoustic waves in periodic systems of metal electrodes on lithium niobate", in *Proc. IEEE Ultrasonics Symposium*, 2003, pp. 2118–2121.

[15] J. Koskela, V. P. Plessky, and M. M. Salomaa, "SAW/LSAW COM parameter extraction from computer experiments with harmonic admittance of a periodic array of electrodes", *IEEE Trans. Ultrason., Ferroelect., Freq. Contr.*, vol. 46, pp. 806–816, 1999.

[16] P. Ventura, J.-M. Hodé, M. Solal, J. Desbois, and J. Ribbe, "Numerical methods for SAW propagation characterization", in *Proc. IEEE Ultrasonics Symposium*, 1998, pp. 175–186.

[17] G. Kovacs, M. Anhorn, H. E. Engan, G. Visintini, and C. C. W. Ruppel, "Improved material constants for $LiNbO_3$ and $LiTaO_3$", in *Proc. IEEE Ultrasonics Symposium*, 1990, pp. 435–438.

[18] T. Makkonen, V. Plessky, V. I. Grigorievski, L. Kopp, M. Solal, W. Steichen, and M. M. Salomaa, "FEM/BEM simulation and experimental study of LLSAW resonator characteristics on YZ-$LiNbO_3$", in *Proc. IEEE Ultrasonics Symposium*, 2002, pp. 305–308.

[19] J. V. Knuuttila, O. Holmgren, T. Makkonen, V. P. Plessky, W. Steichen, and M. M. Salomaa, "Imaging of acoustic fields generated in a longitudinal leaky SAW resonator", in *Proc. IEEE Ultrasonics Symposium*, 2003, pp. 617–620.

[20] T. Pastureaud, S. Ballandras, and W. Steichen, "Prediction of the thermal sensitivity of surface acoustic waves excited under a periodic grating of electrodes", in *Proc. IEEE Ultrasonics Symposium*, 2003, pp. 200–203.

[21] T. Makkonen, V. P. Plessky, W. Steichen, and M. M. Salomaa, "Surface-acoustic-wave devices for the 2.5–5 GHz frequency range based on longitudinal leaky waves", *Appl. Phys. Lett.*, vol. 82, pp. 3351–3353, 2003.

[22] T. Makkonen, V. P. Plessky, W. Steichen, S. Chamaly, C. Poirel, M. Solal, and M. M. Salomaa, "Properties of LLSAW on YZ-cut $LiNbO_3$: Modeling and experiment", in *Proc. IEEE Ultrasonics Symposium*, 2003, pp. 613–616.

[23] T. Makkonen, V. P. Plessky, W. Steichen, S. Chamaly, C. Poirel, M. Solal, and M. M. Salomaa, "Fundamental mode 5 GHz surface-acoustic-wave filters using optical lithography", *Appl. Phys. Lett.*, vol. 83, pp. 3596–3598, 2003.

[24] M. Ylilammi, J. Ellä, M. Partanen, and J. Kaitila, "Thin film bulk acoustic wave filter", *IEEE Trans. Ultrason., Ferroelect., Freq. Contr.*, vol. 49, no. 4, pp. 535–539, 2002.

[25] R. Holland, "Representation of dielectric, elastic, and piezoelectric losses by complex coefficients", *IEEE Trans. Sonics Ultrasonics*, vol. SU-14, pp. 18–20, 1967.

[26] M. Solal, V. Plessky, R. Lardat, T. Makkonen, T. Pastureaud, W. Steichen, and M. M. Salomaa, "Existence of harmonic metal thickness mode propagation for longitudinal leaky waves", in *Proc. IEEE Ultrasonics Symposium*, 2004, pp. 1207–1212.